

Electronic Supporting Information

Photoelectrochemical Reduction of Aqueous Protons With a CuO|CuBi₂O₄ Heterojunction Under Visible Light Irradiation

Hyun S. Park, Chong-Yong Lee, Erwin Reisner*

Christian Doppler Laboratory for Sustainable SynGas Chemistry, Department of Chemistry, University of
Cambridge, Lensfield Road, Cambridge CB2 1EW, United Kingdom.

E-mail: reisner@ch.cam.ac.uk

Contents

Experimental Section	page S2
References	page S4
Supporting Figures	page S5

Experimental Details

Chemicals. $\text{Bi}(\text{NO}_3)_3 \cdot 5\text{H}_2\text{O}$ (98%), ethyl viologen diperchlorate (EV^{2+} , 98%), tetrabutylammonium hexafluorophosphate (TBAPF_6 , 98%), K_2SO_4 (99%), and isopropyl alcohol (99.5%) were purchased from Sigma-Aldrich and were used as received. $\text{Cu}(\text{NO}_3)_2 \cdot 3\text{H}_2\text{O}$ (95%, Fisons PLC.), acetonitrile (MeCN, HPLC grade, Fisher Scientific Ltd.), K_2PtCl_4 (99%, Precious Metals Online Ltd.), KH_2PO_4 (99.5%, Hopkin & Williams Ltd.), K_2HPO_4 (98%, Alfa Aesar), ethylene glycol (Breckland Scientific Supplies Ltd.), and Pt wire (99.997%, 0.1 mm diameter, VWR International Ltd.) was used as received. Milli-Q water (18 M Ω cm) was used as a solvent for the electrochemical experiments. Silver loaded epoxy adhesive (RS Components Ltd.) was used to make electrical contact to the electrodes. Fluorine-doped tin oxide (FTO) glass (TEC 7, $\sim 7 \text{ ohm sq}^{-1}$, Sigma-Aldrich) was used as a conducting substrate for the photoelectrodes.

Electrode preparation. CuO and CuBi_2O_4 thin film electrodes were prepared by drop casting the precursor solution onto FTO-coated glass. Briefly, 10 mM $\text{Cu}(\text{NO}_3)_2 \cdot 3\text{H}_2\text{O}$ (for CuO) or 2 mM $\text{Cu}(\text{NO}_3)_2 \cdot 3\text{H}_2\text{O}$ and 4 mM $\text{Bi}(\text{NO}_3)_3 \cdot 5\text{H}_2\text{O}$ (for CuBi_2O_4) precursor chemicals were prepared in ethylene glycol solution. Then, 150 μL of the precursor solution was applied onto FTO ($1 \times 2 \text{ cm}^2$) preheated at 150 $^\circ\text{C}$ in air. In order to form thin film electrodes with varied thickness, multiple coats of the precursor chemicals were done with a solution drying for 30 min at 150 $^\circ\text{C}$ between the coats. After the repeated drop casts, the precursor film was annealed at 500 $^\circ\text{C}$ for 3 h in air with a ramp rate of 1 $^\circ\text{C min}^{-1}$ from 150 to 500 $^\circ\text{C}$. Then the metal oxide film was slowly cooled down to room temperature before it was characterized.

Instruments. X-ray diffraction (Empyrean, PANalytical B.V.), scanning electron microscopy (LEO Gemini 1530VP), and energy dispersive X-ray spectroscopy (SEM XL30 SFEG) was conducted to study the crystal structure, surface morphology, and atomic elements of the photoelectrodes. A CompactStat.e potentiostat (Ivium Technologies B.V.) was used for the electrochemical experiments including electrochemical impedance spectroscopy (EIS) in a three electrode configuration. A Ag/AgCl reference electrode in a saturated KCl solution and glassy-carbon (GC) rod counter electrode were used for

electrochemical experiments in aqueous solution. A silver wire as a quasi-reference electrode ($\text{EV}^{2+}/\text{EV}^+$ Ag QRE, -0.449 V vs. NHE)¹ and GC counter electrode were used for electrochemical measurements in non-aqueous solution. The AC amplitude for EIS measurements was 10 mV. Illumination (Newport 150 W solar light irradiator) was performed with an AM 1.5G filter and the UV-vis light intensity was 100 mW cm^{-2} . A UV-cutoff filter (420 nm) and monochromator (MSH-300, LOT Quantum design) was used for the visible and monochromatic light irradiation (front-side illumination). A box furnace (EFL, Carbolite Ltd.) was used to anneal the metal oxide films in air.

Photodeposition of electrocatalyst on photocathodes. In order to study the photocathodes in aqueous solution, an electrocatalyst layer was photodeposited not only to improve the HER kinetics, but also to protect the unstable photocathodes from the degradation in aqueous solution. A Pt electrocatalyst was photodeposited onto the electrodes in 10 mM K_2PtCl_4 , 100 mM TBAPF_6 , 8 M H_2O solution using MeCN as a solvent. Briefly, the photocathodes were placed in the deaerated precursor solution followed by chronopotentiometric deposition with a current density of $20 \mu\text{A cm}^{-2}$ under UV-vis light irradiation. The amount of electrocatalyst deposited was controlled by deposition time ranging from 5 to 30 min corresponding to 30 to 180 nmol cm^{-2} of metal precursor reduced at the photocathodes. The stability of platinized photocathode with different Pt loadings was studied in aqueous solution using CA under irradiation. The optimum amount of Pt deposited on the photoelectrodes to produce a stable photocurrent in CA measurements was approximately 90 nmol cm^{-2} of Pt.

Electrochemical detection of hydrogen produced at photocathode. A Pt ultramicroelectrode (UME) was prepared using a Pt wire with a diameter of 100 μm insulated by non-conducting epoxy adhesive (Epoxy Plus 25, Devcon) inside a plastic tube with a diameter of ~ 8 mm. The Pt UME was insulated by the epoxy resin dried overnight at room temperature, followed by electrode polishing using alumina powder. When the hydrogen produced at the photocathode diffuses to the Pt UME, a hydrogen oxidation reaction (HOR) current is detected at the Pt UME while the hydrogen evolution reaction

(HER) current is observed at the photocathode. The time (t_D in s) required for hydrogen diffusion to the Pt UME from the photocathode can be estimated by equation (1).

$$L = (2D_{Ht_D})^{0.5} \quad (1)$$

where D_H is the diffusion coefficient of hydrogen in water, i.e. $4.5 \times 10^{-5} \text{ cm}^2 \text{ s}^{-1}$ at 25°C ,² and L is the distance between the photocathode and the Pt UME in cm.

Calculation of quantum efficiency and integrated photocurrent. The incident photon to current conversion efficiency (IPCE) and the integrated photocurrent over the incident light wavelength (IPCW) was calculated as follows:

$$\text{IPCE}(\lambda) = j(\lambda)/P(\lambda) \times hc/e \lambda \times 100 (\%) \quad (2)$$

$$\text{IPCW}(\lambda) = \frac{\int_{\lambda_0}^{\lambda} \frac{\text{IPCE}(\lambda)}{100} \times \frac{e\lambda P(\lambda)}{hc} d\lambda}{\int_{\lambda_0}^{\lambda_1} \frac{\text{IPCE}(\lambda)}{100} \times \frac{e\lambda P(\lambda)}{hc} d\lambda} \times 100 (\%) = \frac{\int_{\lambda_0}^{\lambda} j(\lambda) d\lambda}{\int_{\lambda_0}^{\lambda_1} j(\lambda) d\lambda} \times 100 (\%) \quad (3)$$

where j [A cm^{-2}] is the photocurrent density measured under the monochromatic light irradiation, P [W cm^{-2}] is the incident light intensity, h [J s] is Planck constant, c [m s^{-1}] is the speed of light, e [C] is the elemental charge, and λ [m] is the wavelength of incident photon. Figure 3 in the main text shows the IPCE and IPCW values under the monochromatic light irradiation with wavelength ranged from 340 (λ_0) to 900 nm (λ_1). The first derivative of IPCW is directly proportional to $\text{IPCE}(\lambda) \times P(\lambda)$ and the absorption spectrum of photoelectrode as shown in Figure 3.

References

1. S. K. Cho, F.-R. F. Fan, A. J. Bard, *Angew. Chem. Int. Ed.* **2012**, *51*, 12740–12744.
2. R. T. Ferrell, D. M. Himmelblau, *AIChE J.* **1967**, *13*, 702–708.

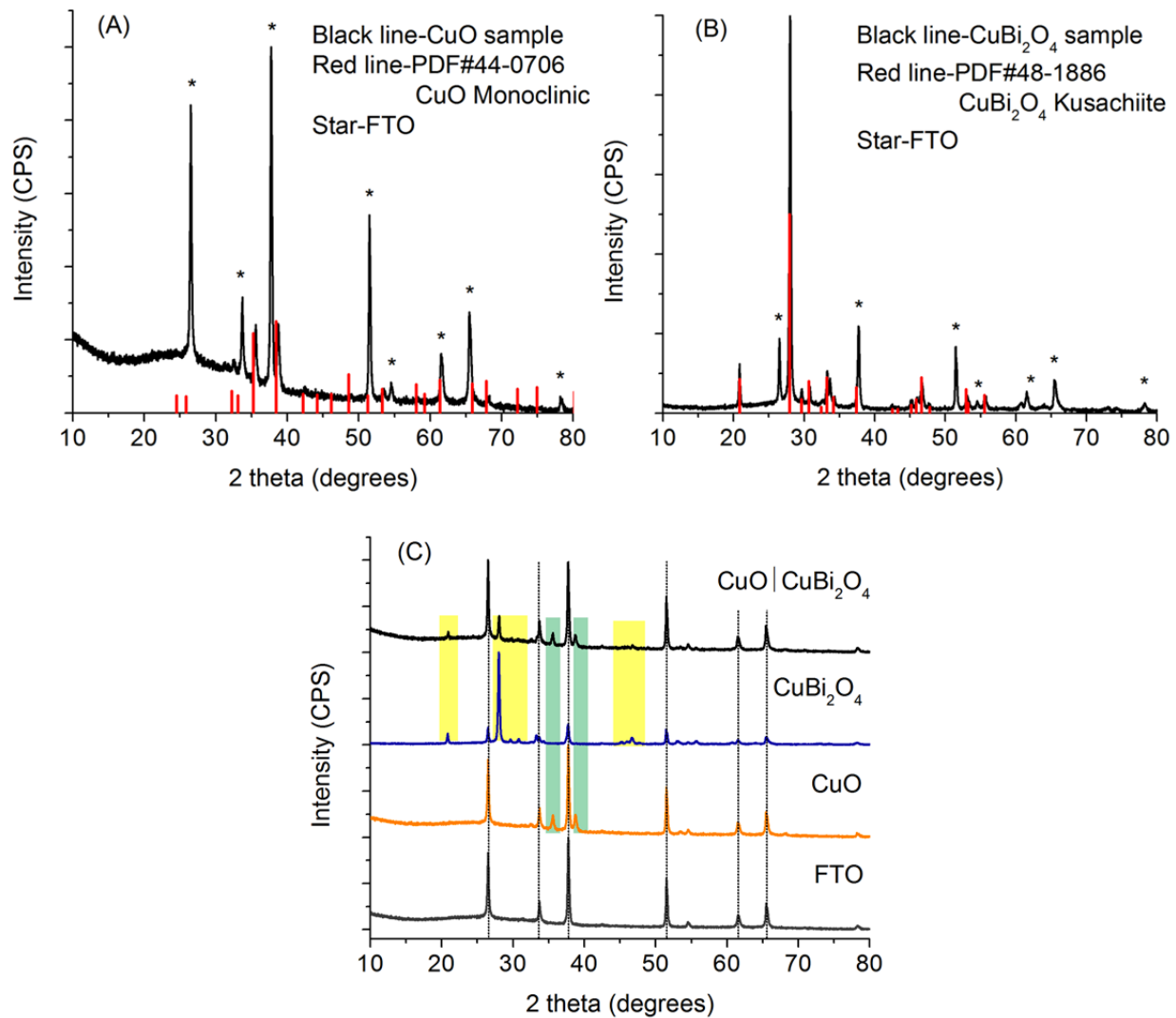


Figure S1. Powder X-ray diffraction patterns of (A) CuO, (B) CuBi₂O₄, and (C) heterojunction of CuO and CuBi₂O₄ in which the patterns from monolayered CuO and CuBi₂O₄ were also included. PDF# stands for the powder diffraction file number.

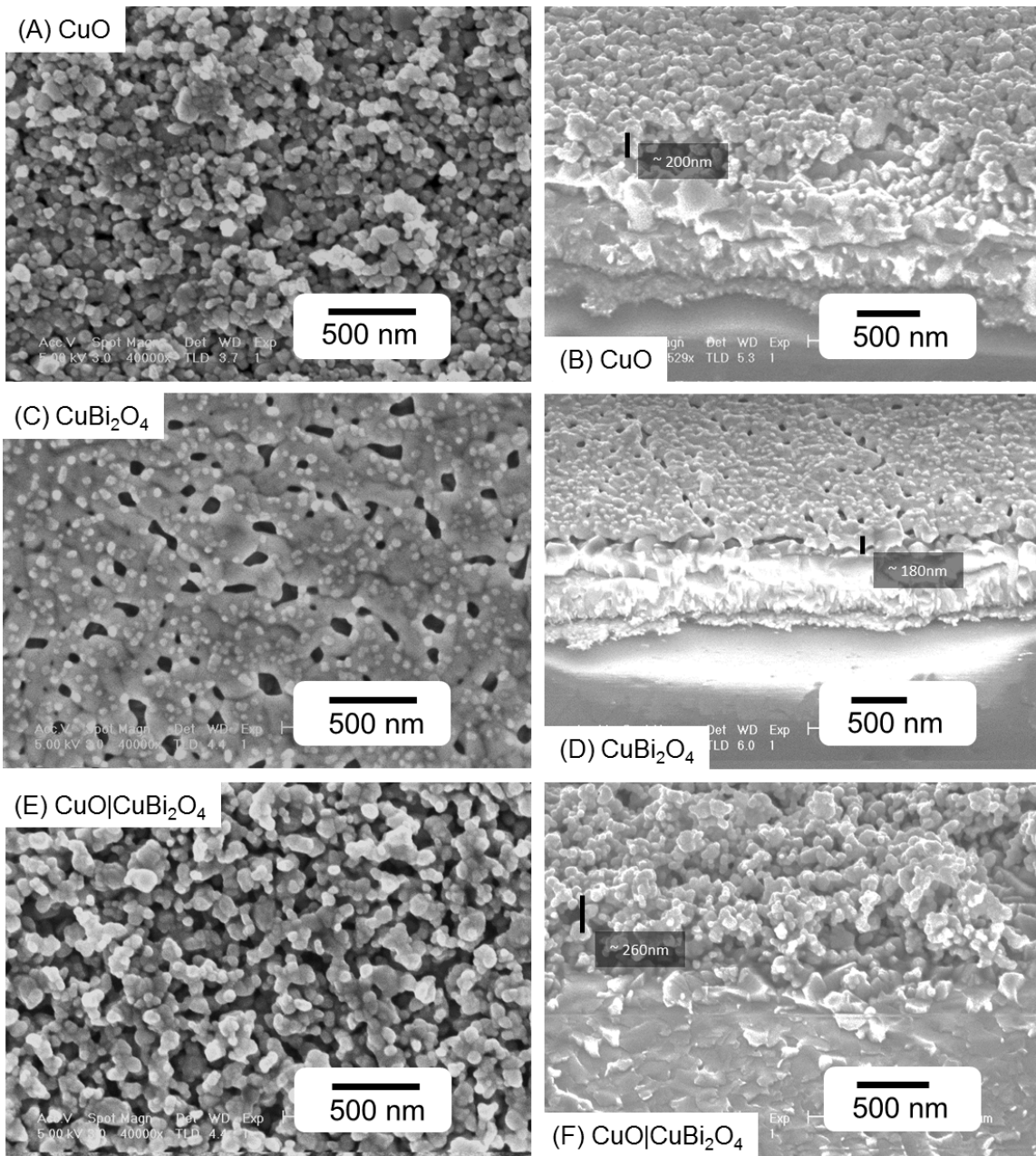


Figure S2. Surface and cross section images of (A and B) CuO, (C and D) CuBi₂O₄, and (E and F) heterojunction of CuO and CuBi₂O₄ obtained by a scanning electron microscopy (SEM).

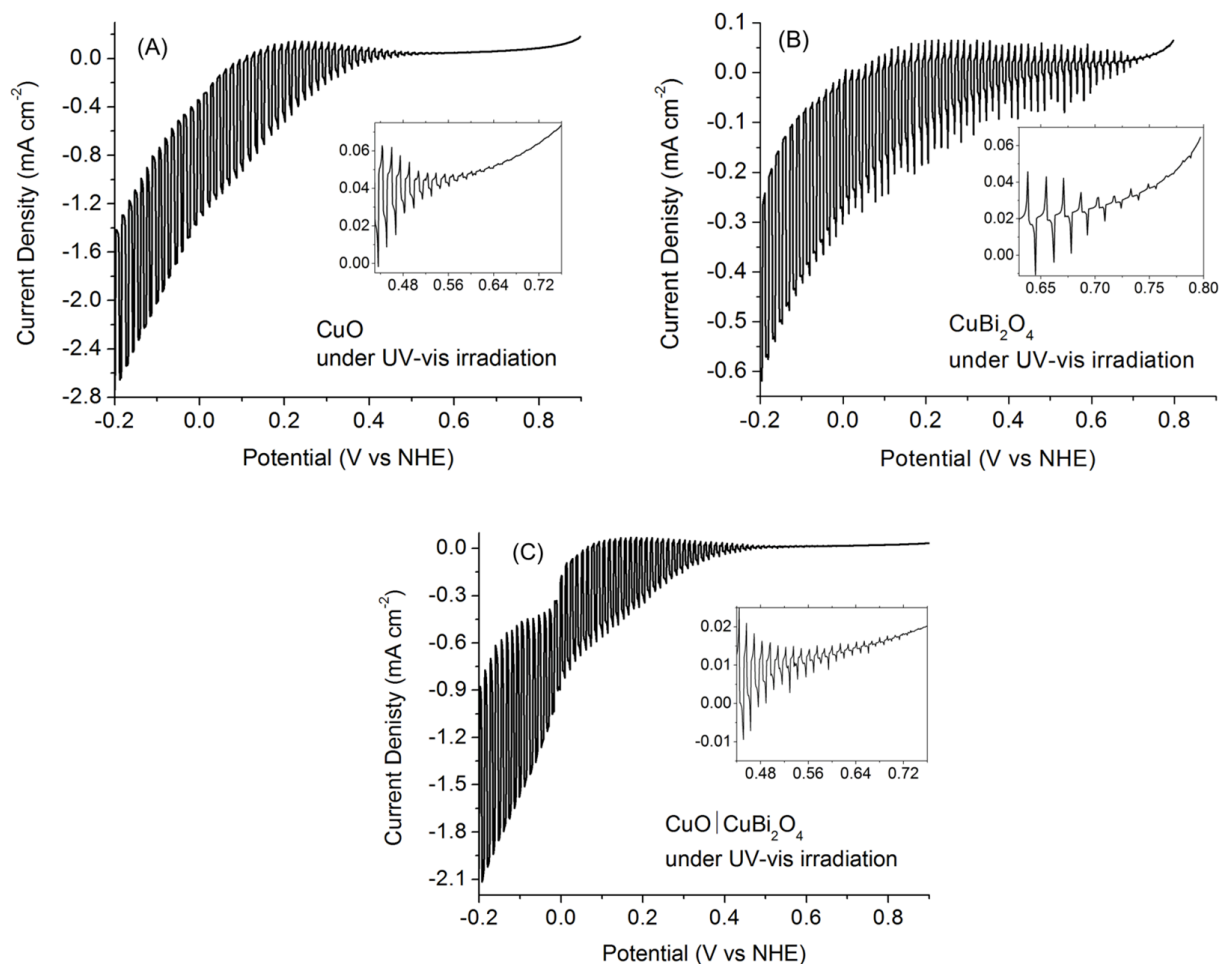


Figure S3. Linear sweep voltammograms (LSVs) of (A) CuO, (B) CuBi₂O₄, and (C) heterojunction of CuO and CuBi₂O₄ measured under chopped UV-vis light irradiation, in pH 6.8 aqueous solution (0.3 M K₂SO₄, 0.1 M phosphate, deaerated) at a scan rate of 20 mV s⁻¹. Insets show the onset potential of the photocurrent. The photocurrent measured in the aqueous solution decreases as the electrode decomposition occurs, and the CuO electrode showed the fastest decay of photocurrent among the photocathodes studied. It is therefore difficult to compare the photoactivities between these unstable electrodes in aqueous electrolyte solution.

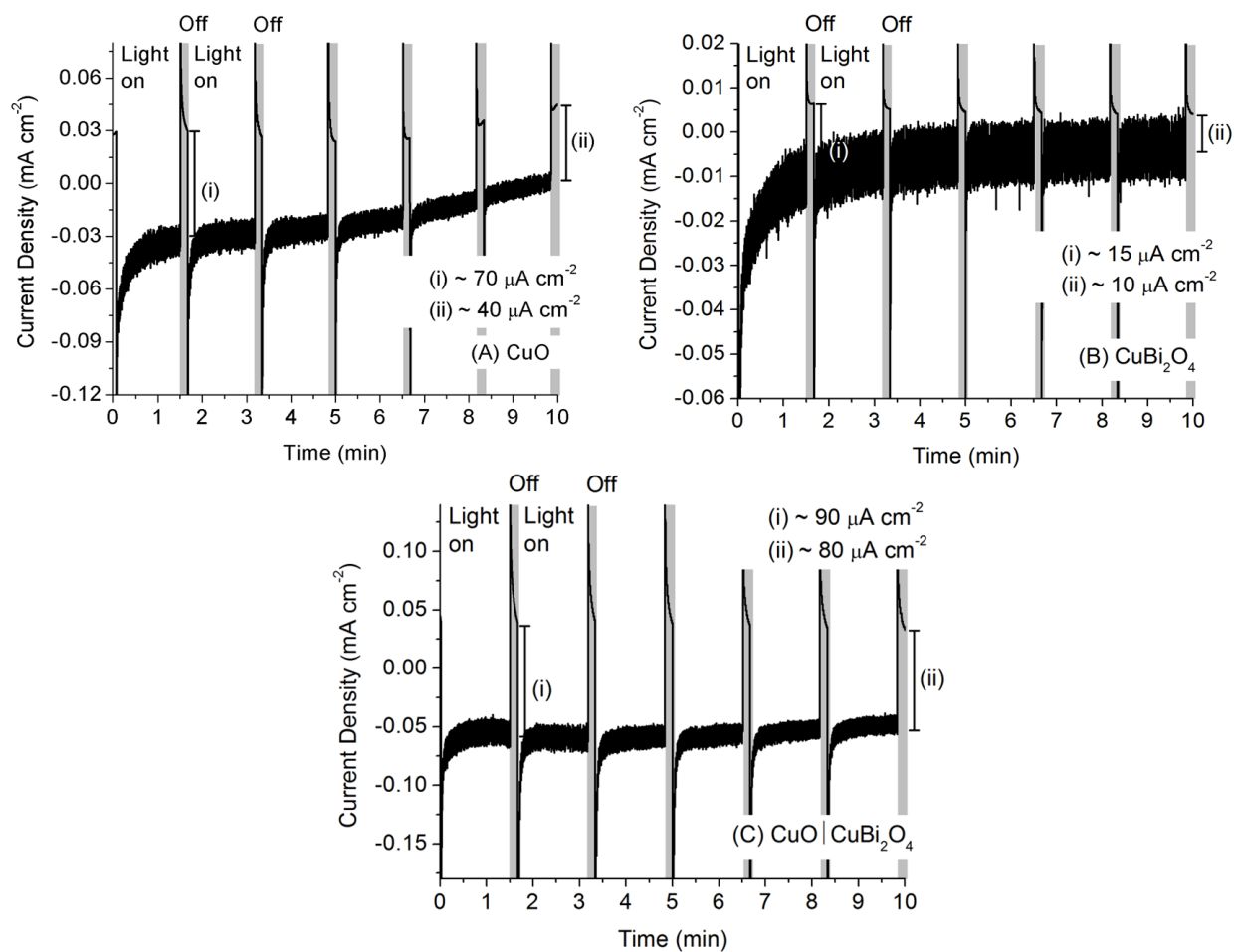


Figure S4. Chronoamperograms of (A) CuO, (B) CuBi₂O₄, and (C) heterojunction of CuO and CuBi₂O₄ measured at 0.2 V vs. NHE under UV-vis irradiation in pH 6.8 aqueous electrolyte solution (0.3 M K₂SO₄, 0.1 M phosphate, deaerated).

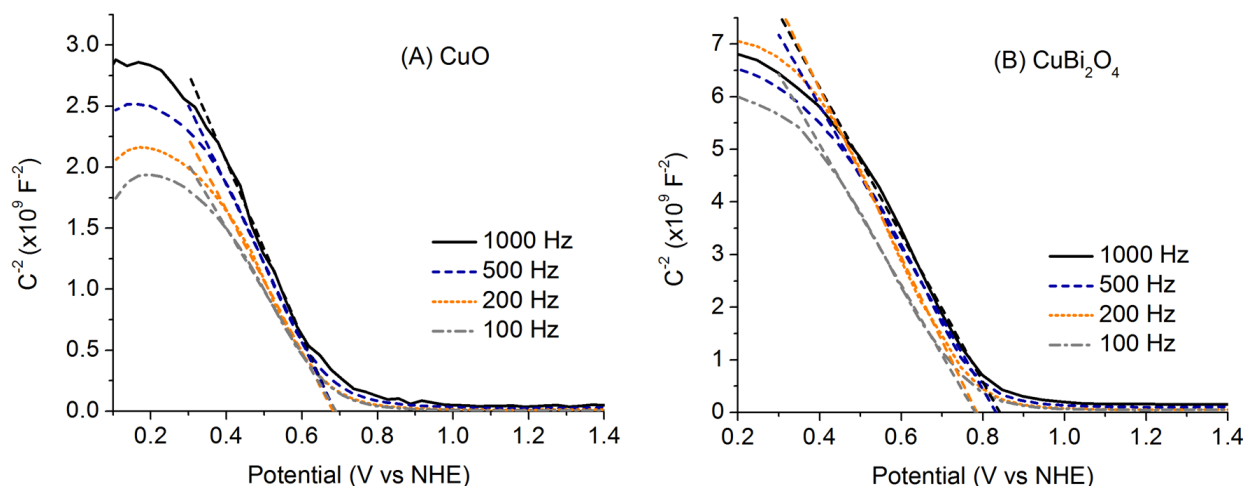


Figure S5. Mott-Schottky plots of (A) CuO and (B) CuBi₂O₄ measured at different frequencies ranged from 100 to 1000 Hz. Tangent lines of the Mott-Schottky plots are added to extrapolate the flat band potential. Measurements were conducted in pH 6.8 aqueous solution (0.3 M K₂SO₄, 0.1 M phosphate).

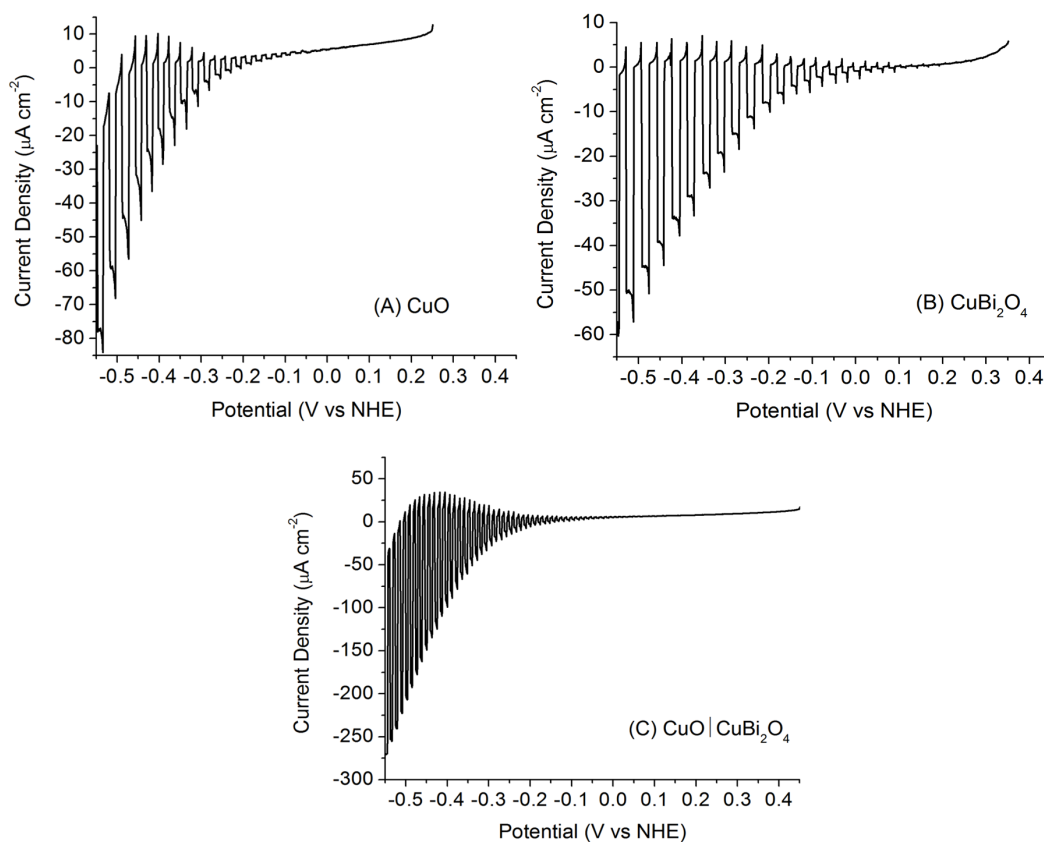


Figure S6. Linear sweep voltammograms of (A) CuO, (B) CuBi₂O₄, and (C) heterojunction of CuO and CuBi₂O₄ recorded under chopped UV-vis light irradiation in EV²⁺ (50 mM) and TBAPF₆ (100 mM) in MeCN at a scan rate of 20 mV s⁻¹.

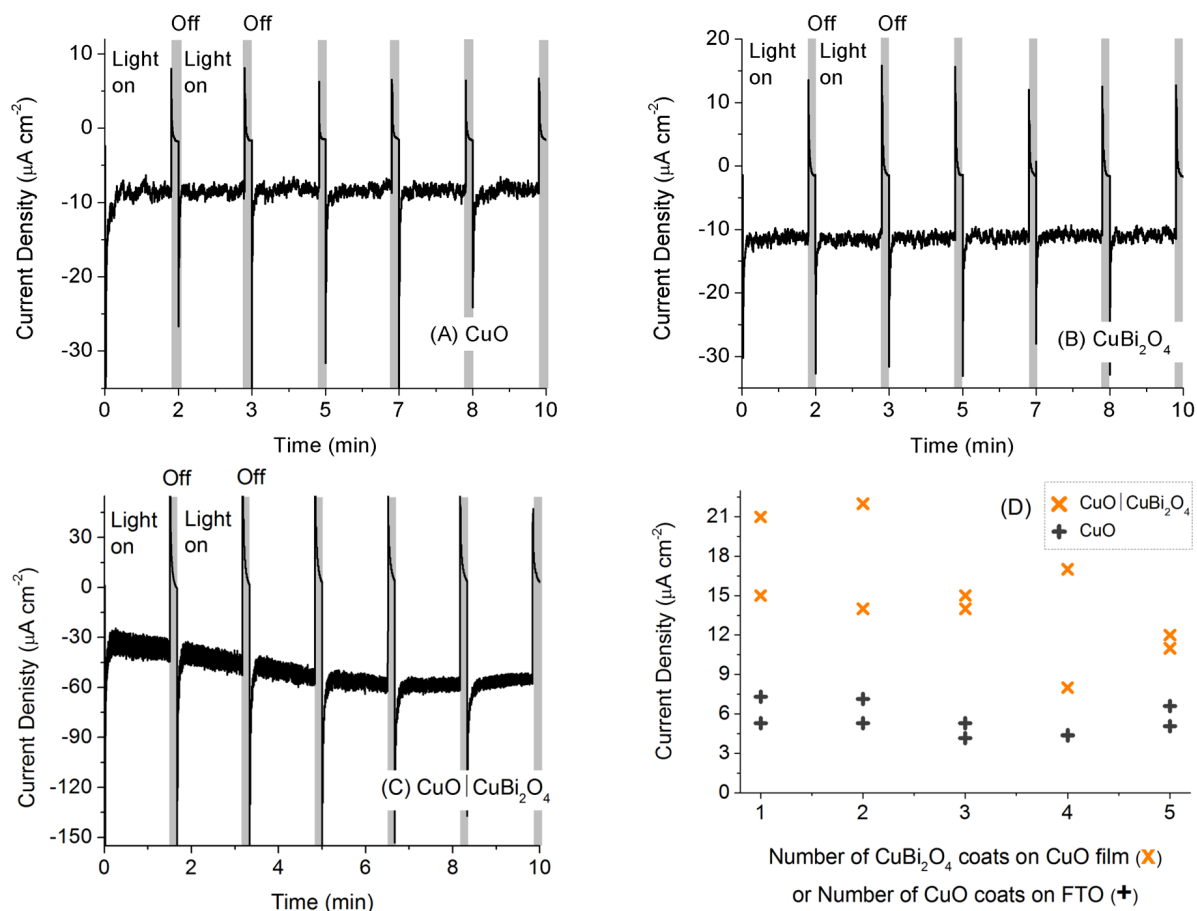


Figure S7. Chronoamperograms of (A) CuO, (B) CuBi₂O₄, and (C) heterojunction of CuO and CuBi₂O₄ measured at -0.45 V vs. NHE under standardized solar light irradiation in EV²⁺ (50 mM) and TBAPF₆ (100 mM) in MeCN. (D) Photocurrent summary with photocathodes for EV²⁺ reduction with different thicknesses measured at -0.45 V vs. NHE in CA (100 mM EV²⁺, 100 mM TBAPF₆ in MeCN). The amount of precursor chemicals drop casted was 0.77 and 0.15 $\mu\text{mol cm}^{-2}$ for CuO and CuBi₂O₄, respectively, for a single coat. The thickness of CuO and CuBi₂O₄ films for a single coat was about 70 and 60 nm, respectively, estimated from cross section SEM images as shown in Figure S2.

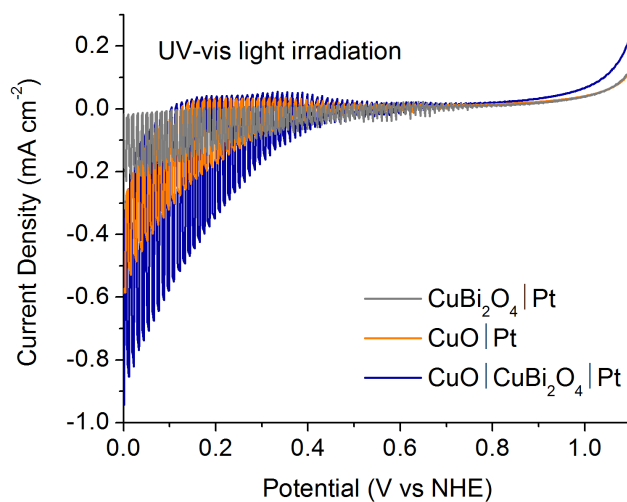


Figure S8. Photocurrent response of FTO|CuO|Pt, FTO|CuBi₂O₄|Pt, and FTO|CuO|CuBi₂O₄|Pt electrodes in pH 6.8 aqueous solution (0.3 M K₂SO₄, 0.1 M phosphate) under Ar at a scan rate of 20 mV s⁻¹ under chopped UV-vis light irradiation.

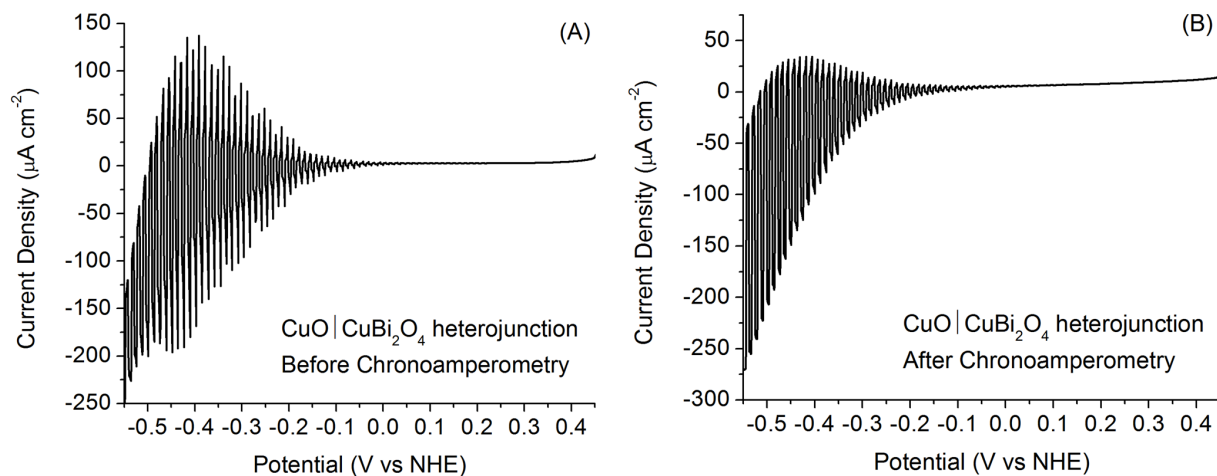


Figure S9. Linear sweep voltammograms (LSVs) of heterojunction of FTO|CuO|CuBi₂O₄ (A) before and (B) after chronoamperometric measurements (Figure S7C) under chopped UV-vis light irradiation in EV²⁺ (50 mM) and TBAPF₆ (100 mM) in MeCN at a scan rate of 20 mV s⁻¹.

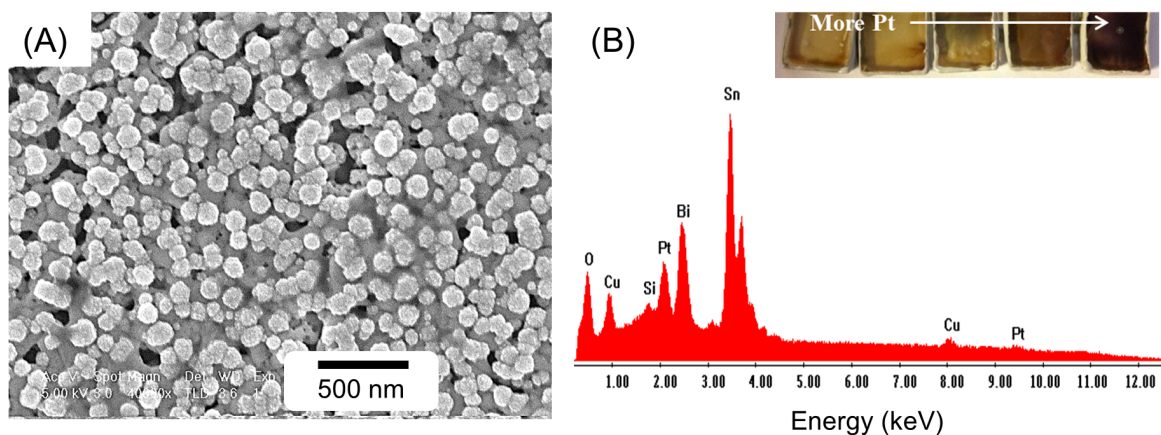


Figure S10. (A) SEM image of $\text{CuBi}_2\text{O}_4|\text{Pt}$ after photodeposition of excess Pt onto CuBi_2O_4 and (B) energy dispersive X-ray spectroscopy of $\text{CuBi}_2\text{O}_4|\text{Pt}$ showing Pt deposited on the film. The inset in (B) shows optical images of photoelectrodes coated with varying amounts of the Pt electrocatalyst.

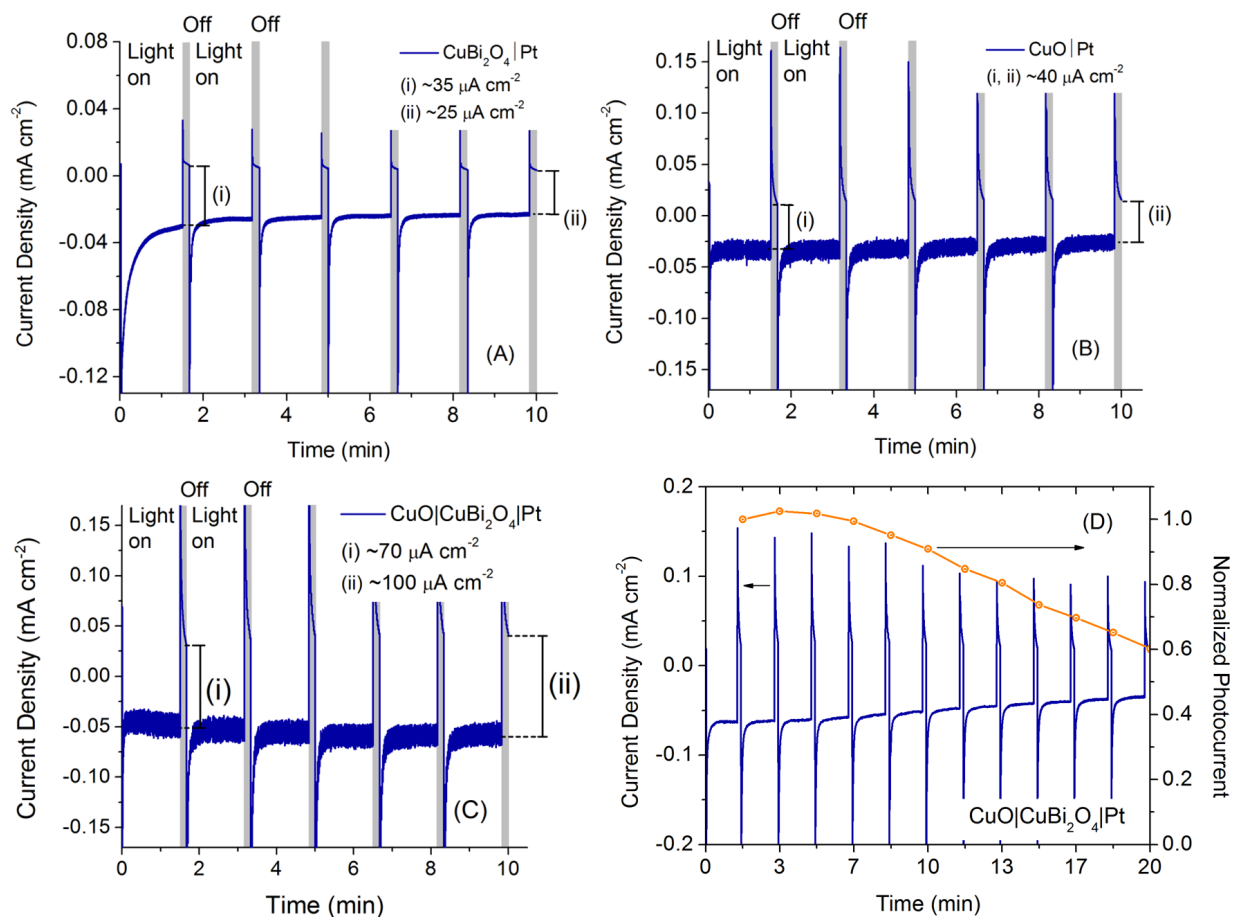


Figure S11. Chronoamperometry runs of (A) $\text{CuBi}_2\text{O}_4|\text{Pt}$, (B) $\text{CuO}|\text{Pt}$, and (C), (D) $\text{CuO}|\text{CuBi}_2\text{O}_4|\text{Pt}$ electrode in pH 6.8 aqueous solution ($0.3 \text{ M K}_2\text{SO}_4$, 0.1 M phosphate, deaerated). (A), (B), and (C) were measured under UV-vis light irradiation, and (D) was under visible light irradiation. CA was measured with an applied potential of 0.2 V vs. NHE.

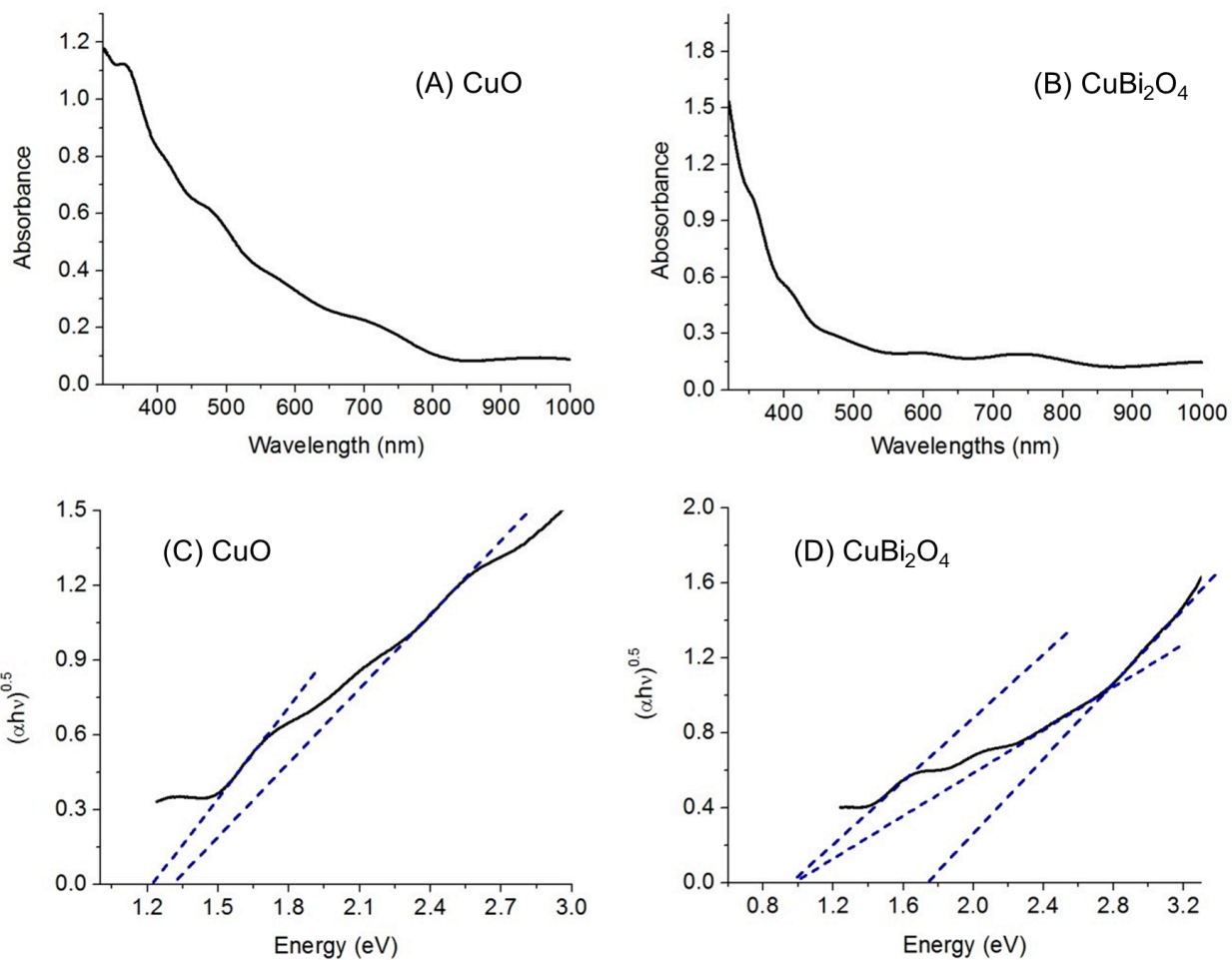


Figure S12. UV-vis absorption spectroscopy of (A) CuO (estimated thickness ~ 70 nm) and (B) CuBi₂O₄ (estimated thickness ~ 200 nm) films deposited on FTO. Tauc plots for indirect band-gap of (C) CuO and (D) CuBi₂O₄ calculated from the UV-vis absorption spectra in (A) and (B).

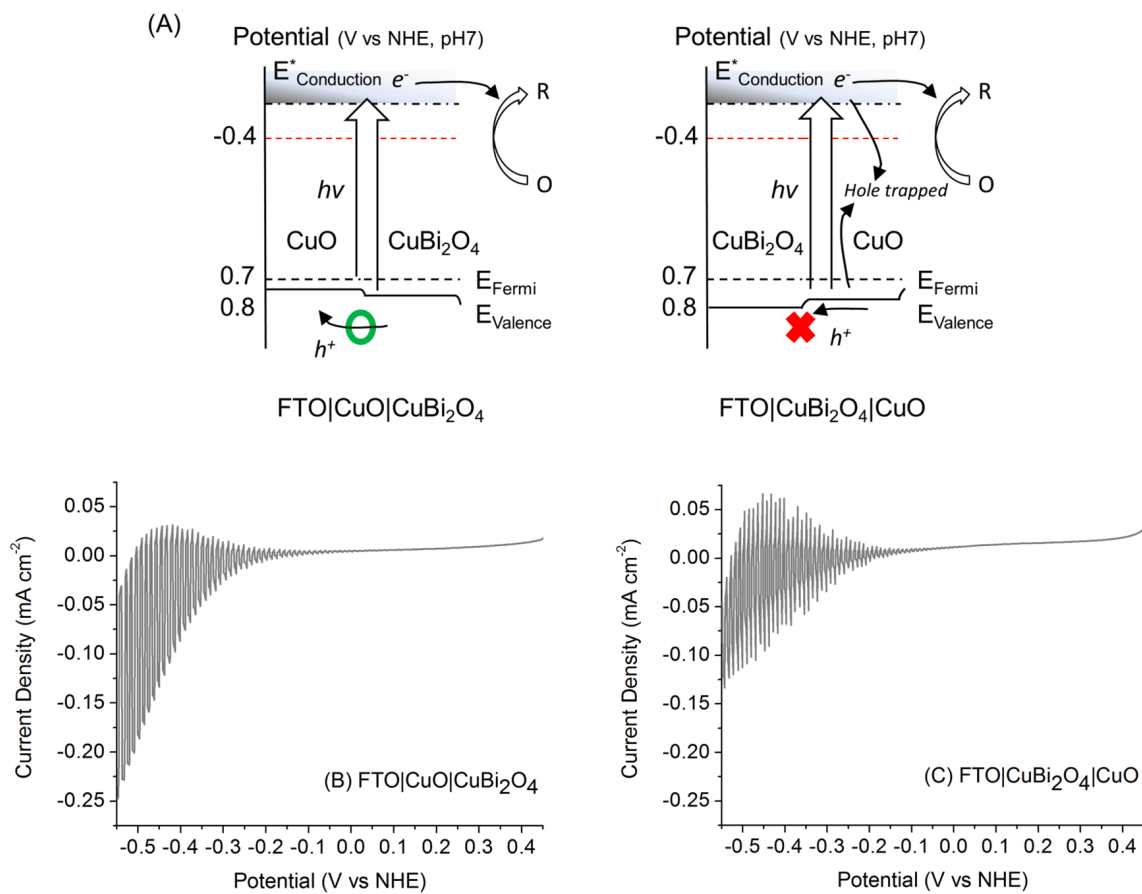


Figure S13. (A) Schematic energy diagram of the estimated band-edge positions of FTO|CuO|CuBi₂O₄ and FTO|CuBi₂O₄|CuO heterojunction electrodes. Linear sweep voltammograms of (B) FTO|CuO|CuBi₂O₄, and (C) FTO|CuBi₂O₄|CuO recorded under chopped visible light irradiation in EV²⁺ (50 mM) and TBAPF₆ (100 mM) in MeCN at a scan rate of 20 mV s⁻¹.

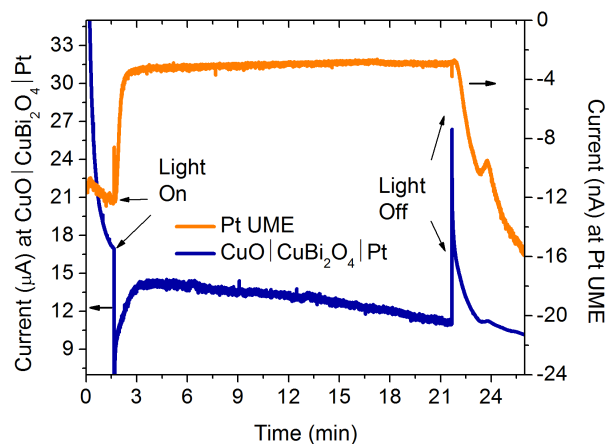


Figure S14. Hydrogen evolution current (HER, blue) and hydrogen oxidation current (HOR, yellow) measured under UV-vis light irradiation of the CuO|CuBi₂O₄|Pt and Pt UME for 20 min in neutral aqueous solution (pH 6.8, 0.3 M K₂SO₄, 0.1 M phosphate, deaerated). CA was measured with an applied potential of 0.2 V vs. NHE to the photocathodes for HER and of -0.3 V vs. NHE to the Pt UME for HOR, respectively.

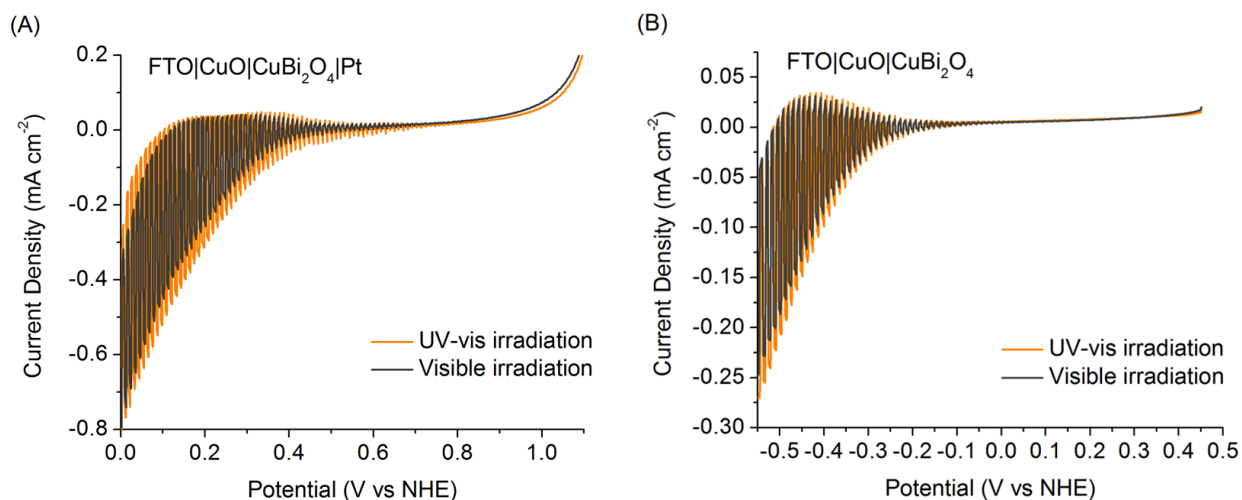


Figure S15. Linear sweep voltammograms of the heterojunction electrode of CuO and CuBi₂O₄ recorded under chopped UV-vis (yellow trace) and visible (grey trace) light irradiation (A) in pH 6.8 aqueous solution (0.3 M K₂SO₄, 0.1 M phosphate) under Ar and (B) in EV²⁺ (50 mM) and TBAPF₆ (100 mM) in MeCN at a scan rate of 20 mV s⁻¹. Pt electrocatalyst was photodeposited onto the electrode for the measurement in aqueous solution.

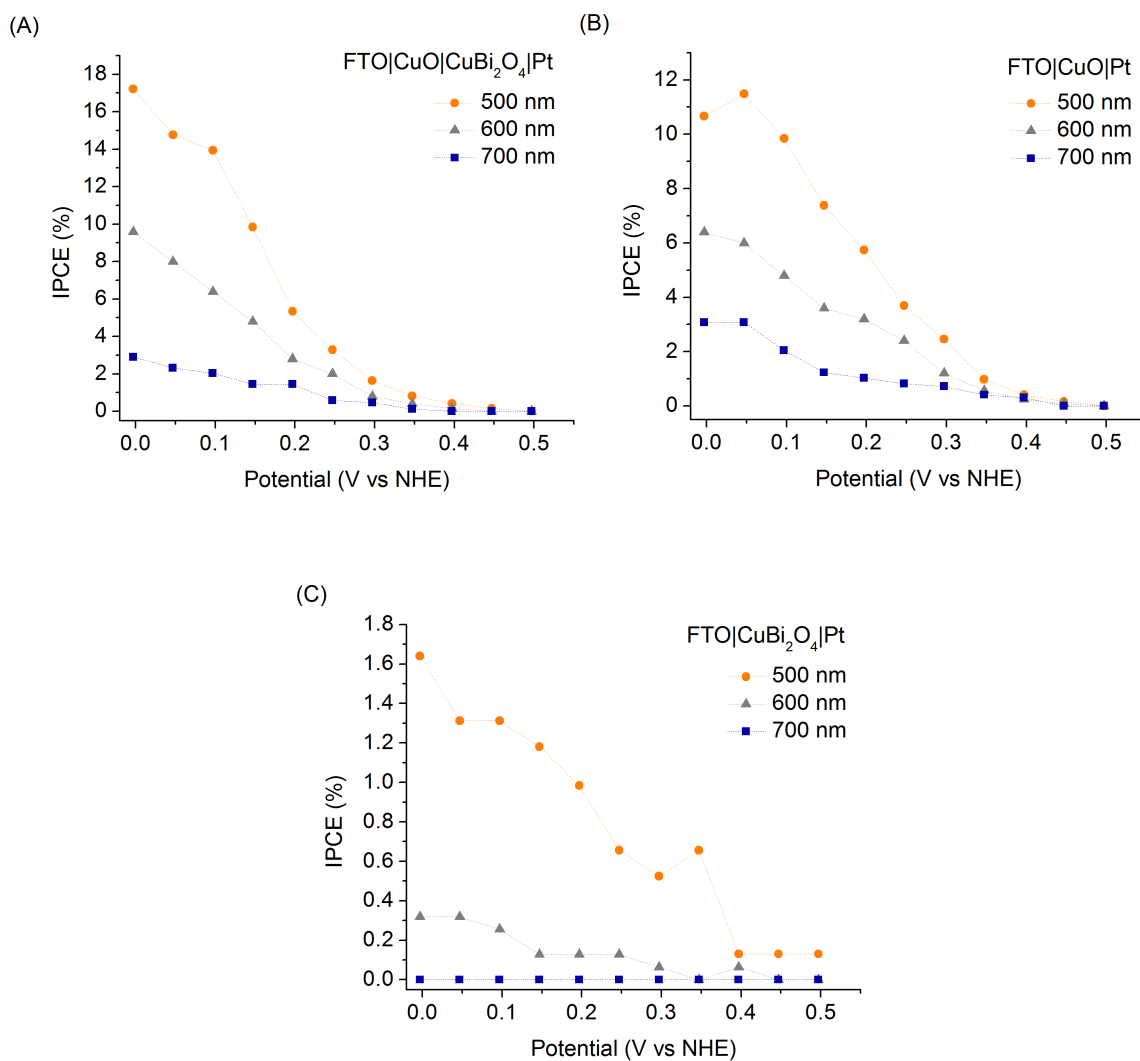


Figure S16. IPCE values at applied potentials of (A) FTO|CuO|CuBi₂O₄|Pt, (B) FTO|CuO|Pt, and (C) FTO|CuBi₂O₄|Pt at different wavelengths (monochromatic light irradiation; 500 nm-orange, 600 nm-gray, and 700 nm-blue). Light intensity was 378, 324, and 216 $\mu\text{W cm}^{-2}$ for the monochromatic light irradiation with a wavelength of 500, 600, and 700 nm, respectively. Photocurrent was recorded in pH 6.8 aqueous solution (0.2 M K₂SO₄, 0.1 M phosphate).

End of Electronic Supporting Information